Equatorial Pacific Warming Attenuated by SST Warming Patterns in the Tropical Atlantic and Indian Oceans

Fosu Boniface (Orcid ID: 0000-0001-7149-4149)
Liguori Giovanni (Orcid ID: 0000-0002-1617-350X)

Equatorial Pacific warming attenuated by SST warming patterns in the tropical Atlantic and Indian Oceans

Boniface Fosu[1], Jie He[1], and Giovanni Liguori[2]

[1]School of Earth and Atmospheric Sciences, Georgia Institute of Technology, Atlanta, USA
[2]School of Earth, Atmosphere and Environment, Monash University, Melbourne, Australia

Corresponding author: Boniface Fosu (boniface.fosu@eas.gatech.edu)

Key points

- Cooling induced by warming in the tropical Indian and Atlantic Oceans significantly reduces the Pacific warming response to increasing GHGs
- Pacific SST response to remote patterns of anthropogenic SST changes is very sensitive to pattern variations among individual models

This article has been accepted for publication and undergone full peer review but has not been through the copyediting, typesetting, pagination and proofreading process which may lead to differences between this version and the Version of Record. Please cite this article as doi: 10.1029/2020GL088231

Abstract

Most climate models project an enhanced mean sea surface temperature (SST) warming in the equatorial Pacific and Atlantic, and a zonal SST dipole in the Indian Ocean. The remote influences of these SST change patterns remain uncertain. To examine the extent to which the patterns of SST changes in the tropical Indian and Atlantic Oceans modulate the warming in the tropical Pacific Ocean, we compare nudging experiments with prescribed structured and uniform SST changes in the tropics outside the Pacific. We find that the warming patterns in the tropical Indian and Atlantic Oceans, respectively, drive a canonical La Niña-like and elongated equatorial cooling through the Bjerknes feedback, acting to attenuate the warming in the equatorial Pacific substantially. The different SST cooling responses emanate from subtle differences between the initial wind forcing driven by the two basins' SST change patterns. These results have significant implications for future climate change projections.

Plain Language Summary

Most of the models that participated in the Coupled Model Intercomparison Project phase 5 (CMIP5) project significant sea surface temperature (SST) warming in the tropics in response to increasing greenhouse gases (GHGs). This projected warming is not uniform in space. The consensus among the CMIP5 models is an enhanced equatorial warming in the Pacific and Atlantic Oceans and an east-west SST dipole in the Indian Ocean. While these warming patterns are well known, their remote influences on long-term tropical SST changes remain uncertain. In this study, we use a climate model to perform simulations in which the patterns of SST changes in the tropical Indian and Atlantic Oceans are prescribed to divulge the extent to which they modulate the warming in the tropical Pacific Ocean. The results show that the warming patterns in the tropical Indian and Atlantic Oceans each induces cooling in the equatorial Pacific, acting together to substantially attenuate the warming there. Such an offset in Pacific SST warming has strong implications for regional climate and climate change projections.

1. Introduction

The warming of the ocean surface from increasing CO_2 exhibits substantial spatial variations. Most models that participated in the Coupled Model Intercomparison Project phase 5 (CMIP5) project an enhanced equatorial warming in the Pacific and Atlantic Oceans and an east-west dipole response in the Indian Ocean (Fig. 1a). These well-documented patterns of SST changes give rise to pronounced changes in both local and remote climate (Vecchi and Soden, 2007; Karnauskas et al., 2009; Xie et al., 2010; He and Soden, 2016; Cai et al., 2019). In particular, the enhanced equatorial warming drives changes in tropical precipitation (Xie et al., 2010) and atmospheric circulation (Ma and Xie 2012; He and Soden, 2015a), alters global teleconnection patterns (Zhou et al. 2014), may increase the frequency of extreme El Niño–Southern Oscillation (ENSO) events (Cai et al., 2014; Zheng et al. 2019) and regulate the magnitude of climate sensitivity (Andrews et al. 2015). Why models project an enhanced equatorial Pacific

warming relative to the global mean warming and whether such a projection is accurate has long been a subject of debate (Seager et al., 2019; Heede et al., 2020).

Several mechanisms within the tropical Pacific basin have been proposed to explain the formation of the projected enhanced equatorial warming. These include the weakening of the Walker circulation and the associated reduction in the upwelling of cold water in the eastern equatorial Pacific (Vecchi and Soden, 2007; Meehl et al., 2007), evaporation-SST feedbacks in the Pacific cold tongue (Knutson and Manabe, 1995; Xie et al., 2010), local cloud feedbacks (DiNezio et al., 2009; Zhang and Li, 2014; Erfani and Burls, 2019) and the advection of subtropical warm water (McCreary and Lu, 1994; Luo et al. 2016). Although the majority of global climate models project enhanced warming in the equatorial Pacific, studies based on simplified models argue that an ocean dynamical thermostat driven by the stratification of upper ocean should reduce the warming in the equatorial Pacific relative to the rest of the tropics (Clement et al., 1996; Cane et al., 1997; Seager and Murtugudde, 1997; Seager et al., 2019). Apart from the advection of subtropical warm water, which is linked to extra-tropical warming and the strength of the Hadley cell driving the Ekman transport, all the aforementioned mechanisms are local to the tropical Pacific Ocean. As to whether the projected warming pattern in the tropical Pacific is influenced by other tropical ocean basins is rather unclear.

It is well known that variations in SST in the tropical Indian and Atlantic Oceans can modulate Pacific SST on interannual and decadal timescales. On interannual timescales, positive tropical equatorial Atlantic SST anomalies in boreal spring can trigger a central Pacific La Niña (Ham et al., 2013; Wang et al., 2017), whereas an equatorial Atlantic Niña in boreal summer can force an eastern Pacific El Niño (Keenlyside and Latif, 2007). Similarly, the leading modes of SST variability in the tropical Indian Ocean, i.e., the Indian Ocean Basin (IOB) and Indian Ocean Dipole (IOD) modes, can influence the Pacific by favoring the onset and demise of El Niño events, respectively.

On decadal to multidecadal timescales, observed SST warming in the tropical Atlantic Ocean can cause stronger trade winds in the Pacific through the modulation of the Walker circulation, leading to a La Niña-like cooling state (McGregor et al., 2014; Li et al., 2015). Other studies have proposed a similar role for the Indian Ocean in causing Pacific trade wind and SST changes (Luo et al., 2012, Zhang et al. 2019). Such decedal interbasin interactions affect the character of ENSO and Pacific decadal variability and was a main contributor to the slowdown of global surface temperature warming at the turn of the last century (Kosaka and Xie, 2013; Trenberth and Fasullo, 2013).

Our study is aimed at divulging how projected patterns of anthropogenic SST changes in remote tropical basins affect Pacific climate, which has hitherto not been done. Specifically, we set out to quantify the degree to which remote patterns of SST changes in the tropical Indian and Atlantic Oceans modulate the tropical Pacific warming from increasing CO_2. The rest of the paper is organized as follows: the model and experimental design are described in section 2. Results are presented in section 3 and are summarized and discussed in section 4.

2. Experimental Design

To quantify the roles of warming patterns in the tropical Indian and Atlantic Oceans in modulating tropical Pacific SST changes under increasing CO_2, we run a suite of nudging and atmosphere-only experiments (e.g., Li et al. 2015) using the Community Earth System Model (CESM1; Hurrell et al., 2013). The atmospheric model component is configured with CAM4 physics on a 1.9° × 2.5° horizontal grid and 26 levels in the vertical, coupled to dynamic ocean (POP2) and sea ice (CICE) models on a nominal horizontal resolution of 1° and 60 vertical levels.

The basic idea of our experiment design is to prescribe spatially patterned and uniform SST warming in the tropical Indian and Atlantic Oceans (i.e., restoring basins), while keeping the rest of the ocean free to evolve under quadruple CO_2 forcing. By comparing the simulations with patterned and uniform warming, the effect of the pattern of SST changes can be investigated. The spatially patterned SST changes in the two restoring basins are taken from the ensemble mean difference between year 121-140 of the abrupt4xCO_2 and control experiments of 21 models that participated in CMIP5 (table S1). For each month, the same spatially patterned and uniform SST changes are repeatedly added to the temporally varying SST from CESM's preindustrial control run to create the forcing data for the nudging and atmosphere-only runs. We add a linearly tapering buffer zone of 9° at the boundaries of the restoring basins (i.e., 23°S-23°N) in order to minimize any artificial SST gradients there. At the start of each simulation, CO_2 is abruptly quadrupled and held constant throughout. Each simulation is integrated for 200 years and the last 180 years are used in our analyses. Fig. S1 shows the temporal mean of the prescribed pattern in the restoring basins.

The design and purpose of all nudging and atmosphere-only simulations are summarized in Table 1. The first pair of nudging (i.e., partially coupled, PC) experiments consist of one with spatially uniform SST changes prescribed in both the tropical Indian and Atlantic Oceans ($PC\_U_I\_U_A$) and one with spatially patterned SST changes prescribed in the same regions ($PC\_P_I\_P_A$). The difference in Pacific SST changes between $PC\_P_I\_P_A$ and $PC\_U_I\_U_A$ reflects the combined impact of the patterns of warming in the tropical Indian and Atlantic Oceans. Similarly, we use the difference between $PC\_P_I\_U_A$ and $PC\_U_I\_U_A$ and that between $PC\_U_I\_P_A$ and $PC\_U_I\_U_A$ to infer the individual influences of the warming pattern of the tropical Indian and Atlantic Oceans, respectively.

The PC experiments are used to reveal the total Pacific response to remote warming patterns, which can be considered as a two-step process: 1) the direct atmospheric response to the remote SST forcing in the restoring basins and 2) the local air-sea coupling in the Pacific initiated by the direct atmospheric response. To dissect them, we perform a set of atmosphere-only simulations, using the atmosphere-land model components of CESM1 (CAM4). The CAM simulations are similar to their nudging counterparts, except that their SST and sea ice conditions are taken from the $PC\_U_I\_U_A$ experiment outside the tropical Indian and Atlantic Oceans (see Table 1). We use $CAM\_P_I\_P_A$ minus $CAM\_U_I\_U_A$, $CAM\_P_I\_U_A$ minus

CAM_U_I_U_A and CAM_U_I_P_A minus CAM_U_I_U_A to identify the direct atmospheric response to the warming pattern in the tropical Indian plus Atlantic Ocean, the tropical Indian Ocean and the tropical Atlantic Ocean, respectively. The effect of local air-sea coupling can be quantified by subtracting the direct atmospheric response (derived from the CAM simulations) from the total response (derived from the PC simulations).

In spite of the lack of two-way ocean-atmosphere coupling in the CAM simulations, the CAM_U_I_U_A and PC_U_I_U_A experiments are statistically indistinguishable (not shown), consistent with He and Soden (2015b). This makes it possible to reasonably discern the secondary response due to the local Pacific air-sea coupling by subtracting the atmosphere-only responses from the coupled responses.

We use the outcome of the PC_U_I_U_A experiment as the baseline to calculate the percent reduction in equatorial Pacific warming due to the pattern of SST changes in the tropical Indian and Atlantic Oceans. First, we establish the Pacific warming pattern in each experiment (Fig. S2), which is given by subtracting the mean of the CESM preindustrial control experiment (i.e., the same control experiment used in creating the surface forcing data for the nudging experiments) over the tropics (30°S-30°N), followed by removing the global mean. The percent reduction in Pacific warming due to SST changes in the tropical Indian and Atlantic basins are then calculated from the ensuing patterns as:

$$\frac{\text{change in equatorial Pacific warming}}{\text{equatorial warming in the PC\_Ui\_Ua experiment}} \text{x } 100$$

Where "change in equatorial Pacific warming" is calculated as the difference in the area averaged equatorial SST (140°E-280°E and 3°S-3°N) between PC experiments with structured warming in the Indian and Atlantic Oceans (i.e., PC_PI_PA, PC_PI_UA and PC_UI_PA) and the PC_Ui_Ua experiment."

Notice that we use the CESM to assess the forced response to the CMIP5 multi-model mean (MMM) pattern of SST changes. This is to provide a baseline depiction and multi-model context of the impact of anthropogenic SST warming patterns in remote tropical basins. Results might change repeating the experiments with a different model (i.e., model-dependent results) or using a single-model pattern rather than the MMM. To demonstrate such model dependencies, we perform a similar set of nudging experiments in which the prescribed pattern of SST changes is taken from the CESM itself. The results are compared to those from the MMM pattern experiments and briefly discussed later in the manuscript.

3. Results

The pattern of SST changes in the tropical Indian and Atlantic Oceans and their remote influences on the tropical Pacific are shown in Fig. 1b – 1d. The combined Indian Ocean and Atlantic SST forcing produces a La Niña-like ocean response accompanied by a band of cooling that emerges off the coast of California, resembling the negative phase of the North Pacific Meridional Mode (NPMM; Chiang and Vimont, 2004). Fig. 1b can be decomposed

further into the Indian Ocean-only (Fig. 1c) and Atlantic-only (Fig. 1d) contributions. Note that the two individual basin contributions add up linearly to the combined response (Fig. 1b). While the band of cooling in the northern subtropical Pacific is largely driven by the Atlantic, both the Atlantic and Indian Ocean induce cooling in the equatorial Pacific surface and subsurface temperature albeit with noticeably different spatial structures. These results remain similar even when we use the last 100 years of our simulations instead of the last 180 years they are presently based on (Fig. S3).

Under the influence of the Indian Ocean, subsurface temperature anomalies in the equatorial Pacific are stronger in the cold tongue region than in the western Pacific (Fig. 1c). The surface response consists of a maximum SST cooling near the eastern boundary and a spatial pattern that resembles the superposition of a negative South Pacific Meridional Mode (SPMM; Zhang et al., 2014; Liguori and Di Lorenzo, 2019) onto a weak La Niña, characterized by a strong zonal SST gradient as shown in Fig. 2a. Unlike the Indian Ocean, the Atlantic Ocean drives somewhat equal cooling in the east and west equatorial Pacific, resulting in a zonally elongated pattern of SST changes that spans the entire equatorial Pacific (Fig. 1d) and a comparatively weak zonal SST gradient (Fig. 2a).

Fig. 2 shows the percent reduction in equatorial Pacific warming due to the pattern of SST changes in the tropical Indian and Atlantic Oceans and summarizes the extent to which the aforementioned remotely forced SST cooling patterns modulate the projected pattern of SST warming in the equatorial Pacific under increasing CO_2. Together, the tropical Indian and Atlantic Oceans account for about a 61% attenuation in the projected pattern of warming of equatorial Pacific SST. The Atlantic-only contribution is about 38% compared to about 29% from the Indian Ocean, making both basins equally important drivers of Pacific SST and climate change. Recall that these SST reduction estimates are relative to the equatorial Pacific warming when uniform SSTs (i.e., average of the prescribed SST pattern in each basin) are prescribed in the tropical Indian and Atlantic basins. It is also noteworthy that the sum of the individual basin contributions is roughly equal to the combined contribution of the two-basin experiment, justifying the linearity assumption (Fig. S4) that is implied by our experimental design.

The cause of the differences between the Indian Ocean and Atlantic induced ocean dynamical responses can be traced to differences in the surface wind responses. Fig. 3 shows the surface wind changes due to direct atmospheric response (middle column), local air-sea coupling (right column) and the sum of the two (i.e., the total response, left column). In the CAM (i.e. atmosphere-only) simulations, SST patterns in the tropical Indian and Atlantic Oceans together drive a Kelvin-wave-induced easterly wind anomaly over the Indo-western Pacific and a weak Rossby-wave-induced westerly wind anomaly in the eastern equatorial Pacific (Fig. 3d). The easterly winds result from the anomalous atmospheric convections driven by the enhanced surface warming in both the Arabian Sea (Fig. 3e) and the equatorial Atlantic (Fig. 3f); while the opposing westerly wind anomaly arises entirely from the warming in the equatorial Atlantic. The underlying ocean responds to the direct wind changes with a La Niña-like dynamical ocean response. The upshot is manifest in the total forced response (Fig. 3a).

Specifically, the atmosphere-only easterly wind anomalies over the Indo-western Pacific strengthen the trade winds, which in turn pushes warm surface waters in the eastern equatorial Pacific westward. This enhances the cold water upwelling in the cold tongue region as well as the equatorial undercurrent (Fig. 1b). The Bjerknes feedback, initiated by a now stronger zonal Pacific SST gradient (Fig. 2a) amplifies this forced response and cools the eastern Pacific in a positive feedback loop (Li et al., 2015).

Both the tropical Indian Ocean (Fig. 3b) and the Atlantic (Fig. 3c) contribute to the total easterly wind anomaly over the Indo-western Pacific (Fig. 3a), with a larger contribution from the Atlantic due to the more intense local air-sea coupling (compare Fig. 3h and 3i). The wind forcing in the Atlantic is congruent with the warm subsurface temperature anomalies in Fig. 1d. In the eastern Pacific, the Atlantic-induced westerly wind anomaly suppresses the anomalous upwelling, which allows the Indian Ocean-induced initial easterly wind response (Fig. 3e), albeit slightly smaller, to produce more cooling (Fig. 1c and 3b) and a greater enhancement in the east-west SST gradient (Fig. 2a). In effect, the subtle differences in the initial wind responses lead to very distinct Pacific responses, i.e., a near-uniform zonally elongated equatorial cooling in the Atlantic experiment and a canonical La Niña-like cooling in the Indian Ocean experiment.

The response due to the local Pacific air-sea coupling is shown in Fig. 3g-i. Overall, the local Pacific air-sea coupling amplifies both the easterly wind anomaly over the Indo-western Pacific, as well as the westerly winds over the eastern equatorial Pacific and the equatorial Atlantic (Fig. 3g). Much of this amplification is driven by the Atlantic (Fig. 3i). In the Indian Ocean realization, the local air-sea coupling slightly alleviates the CAM easterly wind response. The increased east-west gradient in the SST response leads to anomalous subduction near the maritime continents, which drives westerlies from the western North Pacific that oppose the initial CAM response (Fig. 3h); thereby marginally offsetting it.

The large-scale circulation changes associated with these wind changes offer further insights into the Bjerknes feedback and why the responses to the local coupling differ between the Indian Ocean and Atlantic realizations (Fig. 4). Deep atmospheric convection associated with warming over both restoring basins lead to an intensification, as well as a westward displacement of the Indo-Pacific Walker cell (Fig. 4a). However, the largest contribution comes from the Atlantic induced local air-sea coupling (Fig. 4i). This largely Atlantic-driven displacement in the total forced response induces anomalous descending motion over the central tropical Pacific that cools the SST and excites a stationary Rossby wave pattern that extends northward to produce a nearly barotropic anticyclone over the subtropical North Pacific (Lyu et al., 2016). The resulting increase in the subtropical Northeastern Pacific trade winds cool the local SST (Fig. 3c and 3i) via the wind-evaporative-SST (WES) feedback (Xie and Philander, 1994), similar to the physical evolution of the NPMM. This subtropical cooling band acts to speed up both the easterlies over the Indo-western Pacific, as well as the westerlies in the eastern equatorial Pacific (Fig. 3i and 4i) and explains why the Atlantic forcing is able to initiate a stronger local coupling in the western and central equatorial Pacific than the Indian Ocean forcing (Fig. 3g and 4g).

4. Summary and Discussion

We have examined the extent to which the patterns of SST changes in the tropical Indian and Atlantic Oceans can modulate the projected enhanced equatorial warming in the Pacific under increased CO_2. We used the CESM1 model to run a suite of nudging experiments, in which the pattern of SST changes in the tropical Indian and Atlantic Oceans were prescribed, while the rest of the coupled climate system evolves freely under abruptly quadrupled CO_2 forcing. A corresponding set of atmosphere-only experiments are performed to dissect the direct atmospheric response to the remote SST forcing and the local air-sea coupling initiated by the direct atmospheric response.

It was found that the projected warming patterns in the tropical Indian Ocean and the tropical Atlantic Ocean can both induce cooling in the equatorial Pacific. This cooling attenuates the projected equatorial warming in the Pacific Ocean by about 61%. The Atlantic-only contribution to this attenuation is about 38% while that of the Indian Ocean is about 29%. Although the Atlantic contribution is larger, the comparable offset by the Indian Ocean is somewhat in contrast with interbasin studies that have suggested a more important role for the Atlantic Ocean (e.g. McGregor et al., 2014). Our results are consistent with recent studies such as Zhang et al. 2019, who also find that warming in the Indian Ocean can effectively reduce the Pacific warming response to anthropogenic greenhouse gases although their study makes use of observed rather than future trends.

The roles of the direct atmospheric response to the remote SST forcing and the subsequent local air-sea coupling were also examined. The warmest regions over the tropical Atlantic and Indian Oceans generate deep convection, which induces a Gill-type circulation response (Gill 1980), consisting of an easterly Kelvin wave anomaly in the Indo-western Pacific and a westerly Rossby-wave anomaly in the eastern Pacific. The differences in this initial wind forcing between the Indian Ocean and Atlantic experiments are subtle, yet they trigger very different SST and subsurface responses. The local air-sea coupling amplifies both the initial atmosphere responses originating from the Atlantic and Indian basins, but the Atlantic-driven circulation change prompts a stronger coupling with the Pacific Ocean by initiating a PMM-like WES feedback.

While this study focused on the CMIP5 multi-model mean (MMM) pattern of SST change, results may vary among individual models due to the fact that their pattern of SST changes may differ from the MMM. To divulge such variations, we performed a similar set of nudging simulations using SST change patterns from the CESM itself. For ease of reference we refer to these as the "CESM experiments," and the previous set of experiments as the "CMIP experiments." In the CESM experiments, the Atlantic drives a cooling pattern in the Pacific that resembles the one induced by the Indian Ocean from the CMIP experiments (Fig. S5). On the other hand, the Indian Ocean experiment produces a weak and statistically insignificant cooling pattern. The differences between the CESM and CMIP experiments are largely due to the differences in the restoring patterns. While the maximum Atlantic warming is located at the

equator in CMIP, it is north of the equator in CESM. Likewise, the CESM warming pattern produced by the CESM in the tropical Indian Ocean, especially south of the equator, is significantly different from the MMM. This shows the sensitivity of the forced response to pattern variations. Different warming patterns in the Indian and Atlantic oceans from model to model may thus play an important role in the spread of projections of Pacific tropical warming among the CMIP models. Further studies are needed to understand tropical interbasin interactions in different individual models.

The equatorial Pacific still warms significantly, especially in the east, in spite of the remote cooling effect of anthropogenic patterns of SST changes in the tropical Indian and Atlantic Oceans. This indicates that the warming mechanisms that emanate locally from the tropical Pacific are stronger than the remote SST influences of the tropical SST changes outside the Pacific (e.g. Vecchi and Soden, 2007; Xie et al., 2010; Luo et al. 2016; Erfani and Burls, 2019). While the majority of global climate models exhibit this enhanced warming in the equatorial Pacific under increasing CO_2, the accuracy of such projections and the exact nature of the local dynamics are subjects of active debate. Seager et al. (2019) for instance reports a cooling response to global warming in the equatorial Pacific that is consistent with the observed trend but opposes most CMIP5 models. Either way, our results show that the effect of long-term nonlocal anthropogenic patterns of SST warming in the tropical Indian and Atlantic Oceans is to cool the equatorial Pacific, nudging it towards the observed trend.

Acknowledgements

The CMIP5 data were accessed through the ESGF data portal (https://esgf-node.llnl.gov/projects/cmip5/). The CESM preindustrial control runs were obtained from http://www.cesm.ucar.edu/experiments/cesm1.0/. THE CESM code, computing and data storage resources, including the Cheyenne supercomputer (doi:10.5065/D6RX99HX), were provided by the Computational and Information Systems Laboratory (CISL) at NCAR. NCAR is sponsored by the National Science Foundation. This research was also supported by research cyberinfrastructure resources and services provided by the Partnership for an Advanced Computing Environment (PACE) at the Georgia Institute of Technology, Atlanta, Georgia, USA.

References

Andrews, T., J. M. Gregory, and M. J. Webb (2015). The dependence of radiative forcing and feedback on evolving patterns of surface temperature change in climate models, J. Clim., 28, 1630–1648.

Cai, W. J., Wu, L. X., Lengaigne, M., Li, T., McGregor, S., Kug, J. S., Yu, J.-Y., Stuecker, M. F., Santoso, A., Li, X., Ham, Y.-G., Chikamoto, Y., Ng, B., McPhaden, M. J., Du, Y., Dommenget, D., Jia, F., Kajtar, J. B., Keenlyside, N., Lin, X., Luo, J.-J., Martín-Rey, M., Ruprich-Robert, Y., Wang, G., Xie, S.-P., Yang, Y., Kang, S. M., Choi, J.-Y., Gan, B., Kim, G.-I., Kim, C.-E., Kim, S., Kim, J.-H., and Chang, P. (2019). Pantropical climate interactions. Science, 363(6430).

Cai, W., et al. (2014). Increasing frequency of extreme El Niño events due to greenhouse warming, Nat. Clim. Change, 4, 111– 116.

Cane, M.A., Clement A.C., Kaplan A., Kushnir Y., Pozdnyakov D., Seager R., Zebiak S.E. and Murtugudde R. (1997). Twentieth-Century Sea Surface Temperature Trends, Science 275, 5302, pp. 957-96.

Chiang, J. C. H., and D. J. Vimont (2004). Analogous Pacific and Atlantic Meridional Modes of tropical atmosphere-ocean variability, J. Clim., 17, 4143– 4158.

Clement, A. C., Seager, R., Cane, M. A., and Zebiak, S. E. (1996). An ocean dynamical thermostat. Journal of Climate, 9(9), 2190–2196.

DiNezio, P. N., Clement, A. C., Vecchi, G. A., Soden, B. J., Kirtman, B. P., and Lee, S.-K. (2009). Climate response of the equatorial Pacific to global warming. Journal of Climate, 22(18), 4873–4892.

Erfani, E., and N. J. Burls (2019). The strength of low-cloud feedbacks and tropical climate: A CESM sensitivity study. J. Climate, 32, 2497–2516.

Gill, A. E. (1980). Some simple solutions for heat-induced tropical circulation. Quarterly Journal of the Royal Meteorological Society, 106(449), 447–462.

Ham Y.-G., Kug J.-S., Park J.-Y., Jin F.-F. (2013). Sea surface temperature in the north tropical Atlantic as a trigger for El Niño/Southern Oscillation events. Nat. Geosci. 6, 112–116.

He, J., and Soden B. J. (2016). The impact of SST biases on projections of anthropogenic climate change: a greater role for atmosphere-only models? Geophys. Res. Lett., 43(14).

He, J., and Soden B. J. (2015a). Anthropogenic weakening of the tropical circulation: the relative roles of direct CO_2 forcing and sea surface temperature change, J. Climate, 28(22), 8728-8742

He, J., and Soden B. J. (2015b). Does the lack of coupling in SST-forced atmosphere-only models limit their usefulness for climate change studies? J. Climate, 29(12), 4317-4325.

Heede, U. K., Fedorov, A. V., and Burls, N. J. (2020). Time scales and mechanisms for the tropical pacific response to global warming: A tug of war between the ocean thermostat and weaker walker. Journal of Climate, 33 (14).

Hurrell, J. W., Holland, M. M., Gent, P. R., Ghan, S., Kay, J. E., Kushner, P. J., et al. (2013). The Community Earth System Model: A framework for collaborative research. Bulletin of the American Meteorological Society, 94(9), 1339–1360.

Karnauskas, K. B., Seager, R., Kaplan, A., Kushnir, Y., and Cane, M. A. (2009). Observed strengthening of the zonal sea surface temperature gradient across the equatorial Pacific Ocean. Journal of Climate, 22(16), 4316–4321.

Keenlyside N. S. and Latif M. (2007). Understanding equatorial Atlantic interannual variability. J. Clim. 20, 131–142.

Kosaka, Y., and Xie, S.-P. (2013). Recent global-warming hiatus tied to equatorial Pacific surface cooling. Nature, 501(7467), 403–407.

Knutson, T. R., and Manabe, S. (1995). Time-mean response over the tropical Pacific to increased CO2 in a coupled ocean-atmosphere model. Journal of Climate, 8(9), 2181–2199.

Li, X., Xie, S.-P., Gille, S. T., and Yoo, C. (2015). Atlantic-induced pan-tropical climate change over the past three decades. Nature Climate Change, 6(3), 275–279.

Liguori, G., and Di Lorenzo, E. (2019). Separating the North and South Pacific Meridional Modes contributions to ENSO and tropical decadal variability. Geophysical Research Letters, 46, 906–915.

Luo, J.-J., Sasaki, W., and Masumoto, Y. (2012). Indian Ocean warming modulates Pacific climate change. Proceedings of the National Academy of Sciences of the United States of America, 109(46), 18,701–18,706.

Luo, Y., Lu, J., Liu, F., and Garuba, O. (2016). The role of ocean dynamical thermostat in delaying the El Niño-like response over the equatorial pacific to climate warming. Journal of Climate, 30 (8), 2811– 2827.

Lyu, K., Yu J.-Y., and Paek H. (2017). The influences of the Atlantic Multidecadal Oscillation on the mean strength of the North Pacific subtropical high during boreal winter, J. Clim., 30, 411– 426

Ma, J., Xie, S.-P., and Kosaka, Y. (2012). Mechanisms for tropical tropospheric circulation change in response to global warming. Journal of Climate, 25(8), 2979–2994.

McCreary, J. P., and Lu, P. (1994). Interaction between the subtropical and equatorial ocean circulations: the subtropical cell. Journal of Physical Oceanography, 24, 466– 497.

McGregor, S., Timmermann, A., Stuecker, M. F., England, M. H., Merrifield, M., Jin, F. F., and Chikamoto, Y. (2014). Recent Walker circulation strengthening, and Pacific cooling amplified by Atlantic warming. Nature Climate Change, 4(10), 888– 892.

Meehl G.A. and Teng H. (2007). Multi-model changes in El Niño teleconnections over North America in a future warmer climate. Clim Dyn. 29:779–90.

Seager, R., and Murtugudde, R. (1997). Ocean dynamics, thermocline adjustment, and regulation of tropical SST. Journal of Climate, 10(3), 521–534.

Seager, R., Cane, M., Henderson, N., Lee, D. E., Abernathey, R., and Zhang, H. (2019). Strengthening tropical Pacific zonal sea surface temperature gradient consistent with rising greenhouse gases. Nature Clim. Change, 9, 517 – 522.

Trenberth, K. E. and Fasullo, J. T. (2013). An apparent hiatus in global warming? Earth's Future 1, 19–32.

Vecchi, G. A., and Soden, B. J. (2007). Global warming and the weakening of the tropical circulation. Journal of Climate, 20(17), 4316–4340.

Wang L., Yu J.-Y., and H. Paek (2017). Enhanced biennial variability in the Pacific due to Atlantic capacitor effect. Nat. Commun. 8,14887.

Xie, S.-P., Deser, C., Vecchi, G. A., Ma, J., Teng, H., and Wittenberg, A. T. (2010). Global warming pattern formation: Sea surface temperature and rainfall. Journal of Climate, 23(4), 966–986.

Xie, S.-P. and Philander, S. G. H (1994). A coupled ocean-atmosphere model of relevance to the ITCZ in the eastern Pacific. Tellus 46A, 340–350.

Zhou Z-Q, Xie S-P, Zheng X-T, Liu Q, Wang H (2014). Global Warming–Induced Changes in El Niño Teleconnections over the North Pacific and North America. *Journal of Climate*, 27(24):9050–9064.

Zhang, L., and Li, T. (2014). A simple analytical model for understanding the formation of sea surface temperature patterns under global warming. Journal of Climate, 27(22), 8413–8421.

Zhang, H., Clement, A., and Di Nezio, P. (2014). The South Pacific Meridional Mode: A mechanism for ENSO-like variability. Journal of Climate, 27(2), 769–783.

Zhang, L., Han, W., Karnauskas, K. B., Meehl, G. A., Hu, A., Rosenbloom, N., & Shinoda, T. (2019). Indian Ocean warming trend reduces Pacific warming response to anthropogenic greenhouse gases: An interbasin thermostat mechanism. Geophysical Research Letters, 46, 10,882–10,890.

Zheng, X. (2019), Indo-Pacific Climate Modes in Warming Climate: Consensus and Uncertainty Across Model Projections. Curr Clim Change Rep 5, 308–321.

Table 1. A summary of all nudging experiments performed in this study and how they are utilized. TIO and TAO are abbreviations for the Tropical Indian Ocean and the Tropical Atlantic Ocean, respectively. Patterns of SST changes are determined from the ensemble mean difference between year 121-140 of the abrupt4xCO_2 and pre-industrial control experiments of 21 CMIP5 models (**Table S1**). Uniform SST in each target basin is calculated as the area-weighted average of its patterned SST.

No	Experiment	Experimental Setup	Rationale and Diagnostics
Nudging experiments (i.e. total response)			
1	PC_U_I_U_A	Prescribed uniform SST changes in the TIO and the TAO. The tropical Pacific is free to evolve	Baseline experiment; used to determine the total response to uniform SST changes in the TIO and the TAO
2	PC_P_I_P_A	Prescribed patterned SST changes in the TIO and the TAO. The tropical Pacific is free to evolve	PC_P_I_P_A *minus* PC_U_I_U_A is used to determine the total response to the patterns of SST changes in the TIO and the TAO (i.e., combined Indian Ocean and Atlantic response)
3	PC_P_I_U_A	Prescribed patterned SST changes in the TIO but uniform SST in the TAO. The tropical Pacific is free to evolve	PC_P_I_U_A *minus* PC_U_I_U_A is used to determine the total response to the pattern of SST changes in the TIO (i.e., Indian Ocean-only response)
4	PC_U_I_P_A	Prescribed uniform SST changes in the TIO but patterned SST in the TAO. The tropical Pacific is free to evolve	PC_U_I_P_A *minus* PC_U_I_U_A is used to determine the total response to the pattern of SST changes in the TAO (i.e., Atlantic-only response)
CAM experiments (i.e. direct atmospheric response)			
5	CAM_U_I_U_A	Uniform SST changes in the TIO and the TAO. Outside the two basins, SST and sea ice are taken from the PC_U_I_U_A experiment	
6	CAM_P_I_P_A	Patterned SST changes in the TIO and the TAO. Outside the two basins, SST and sea ice are taken from the PC_U_I_U_A experiment	CAM_P_I_P_A *minus* CAM_U_I_U_A is used to determine the initial atmosphere only response to the patterns of SST changes in the TIO and the TAO
7	CAM_P_I_U_A	Patterned SST changes in the TIO and spatially uniform SST in the TAO. Outside the two basins, SST and sea ice are taken from the PC_U_I_U_A experiment	CAM_P_I_U_A *minus* CAM_U_I_U_A is used to determine the atmosphere only response to the pattern of SST changes in the TIO
8	CAM_U_I_P_A	Uniform SST changes in the TIO and patterned SST in the TAO. Outside the two basins, SST and sea ice are taken from the PC_U_I_U_A experiment	CAM_U_I_P_A *minus* CAM_U_I_U_A is used to determine the atmosphere only response to the pattern of SST changes in the TAO
Further Diagnostics			**Rationale**
Effect of local air-sea coupling (i.e. total response – direct atmospheric response)			
9	[PC_P_I_P_A – PC_U_I_U_A] *minus* [CAM_P_I_P_A – CAM_U_I_U_A]		To isolate the effects of the local Pacific air-sea coupling initiated by the direct atmospheric response to the warming patterns in the TIO and the TAO
10	[PC_P_I_U_A – PC_U_I_U_A] *minus* [CAM_P_I_U_A – CAM_U_I_U_A]		To isolate the effects of the local Pacific air-sea coupling initiated by the direct atmospheric response to the warming pattern in the TIO
11	[PC_U_I_P_A – PC_U_I_U_A] *minus* [CAM_U_I_P_A – CAM_U_I_U_A]		To isolate the effects of the local Pacific air-sea coupling initiated by the direct atmospheric response to the warming pattern in the TAO
Percent reduction in equatorial Pacific SST			
12	$\frac{\text{Change in equatorial Pacific warming}}{\text{Equatorial warming in the PC\_UI\_Ua experiment}} \times 100$ Change in equatorial Pacific warming is calculated as the difference in the area averaged equatorial SST (140E-280E and 3S-3N) between the PC_UI_Ua experiment and the PC_PI_PA, PC_PI_UA and PC_UI_PA experiments.		To determine the percent reduction in equatorial Pacific SST due to the pattern of SST changes in the TIO and the TAO. The PC_U_I_U_A experiment is used as the baseline for the reduction.

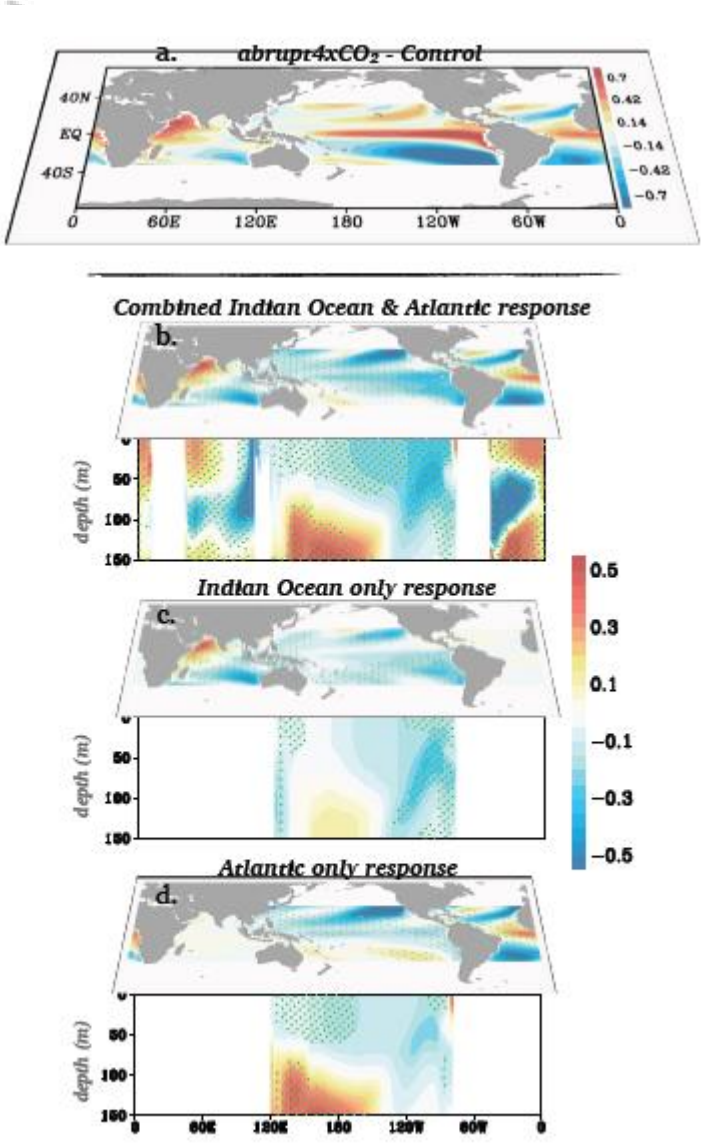

Figure 1. (a) Pattern of SST changes under increasing CO_2; determined by taking the ensemble mean difference between year 121-140 of the abrupt4xCO_2 and control experiments of 21 CMIP5 models (Table S1). The spatial average of each pattern has been subtracted. **(b-d)** Pacific SST and subsurface potential temperature (averaged from 5°S-5°N) changes induced by the tropical Indian and Atlantic Oceans combined (i.e., PC_P_I_P_A - PC_U_I_U_A), the Indian Ocean only (i.e., PC_P_I_U_A - PC_U_I_U_A) and the Atlantic Ocean only (i.e., PC_U_I_P_A - PC_U_I_U_A). Green stippling show statistically significant changes at the 90% confidence level based on the Student's t-test. The same color bar applies to all plots from b-d. Unit is °C. See Table 1 for further details on how the Indian Ocean and Atlantic driven responses are obtained.

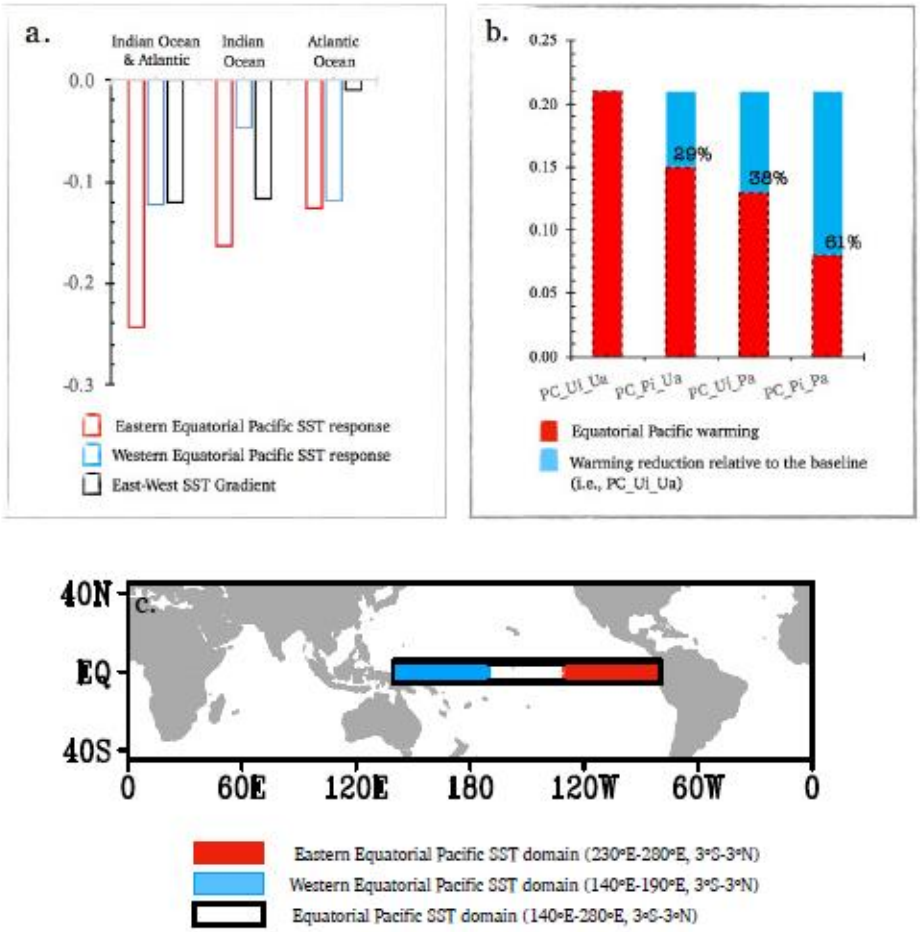

Figure 2. (a) The east-west gradient in the equatorial Pacific SST response (based on Fig. 1 b-d): the red bars represent the area-averaged SST response of the western equatorial Pacific (i.e., 140°E-190°E, 3°S-3°N) while blue outlines represent the area-averaged SST response of the eastern equatorial Pacific (i.e., 230°E-280°E, 3°S-3°N). The east-west SST gradients (east-minus-west) are shown in black outlines. **(b)** The extent to which the tropical Indian and Atlantic Oceans can remotely modulate equatorial Pacific SST: the red bars represent the area-weighted average of equatorial Pacific warming (140°E-280°E, 3°S-3°N). The equatorial Pacific warming (Fig. S2) in each experiment, is obtained by subtracting the temporal mean of the CESM preindustrial control experiment (used in creating the surface forcing data for the nudging experiments) over the tropics (30°S-30°N), followed by removing the global mean. The blue bars represent the warming reduction in $PC\_P_I\_P_A$ (i.e., the combined Indian Ocean and Atlantic experiment) $PC\_P_I\_U_A$ (i.e., the Indian Ocean only experiment), and $PC\_U_I\_P_A$ (i.e., the Atlantic only experiment) relative to $PC\_U_I\_U_A$ (i.e., the baseline warming experiment). The corresponding percent reductions in equatorial Pacific SST are superimposed. See **Table 1** for further details. **(c)** The SST domains based on which the metrics in **(a)** and **(b)** are calculated are provided for ease of reference. All units are in °C.

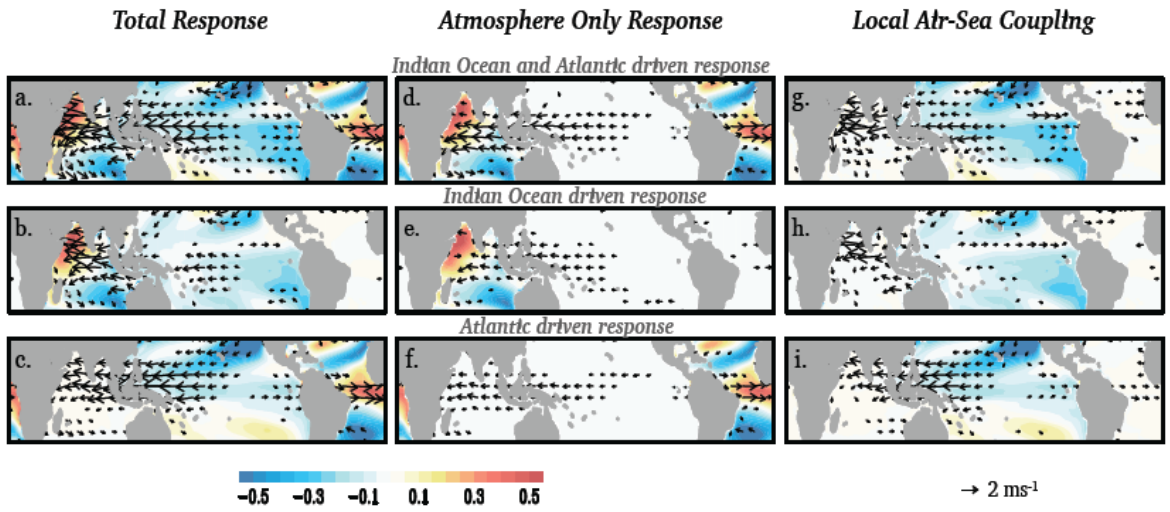

Figure 3. The mean SST (shading, °C) and 850 hPa winds (vectors, ms^{-1}) changes in the **(a-c)** partially coupled CESM run (i.e., total response), **(d-f)** CAM run (i.e., atmosphere only response) and **(g-i)** the difference between them (i.e., partially coupled – CAM; local air-sea coupling). Only statistically significant wind vectors at the 90% confidence level are plotted. Statistical significance is based on the Student's t-test. The arrow scale on the bottom right hand side of the figure applies to all plots. See **Table 1** for further details on how the Indian Ocean and Atlantic driven responses are obtained.

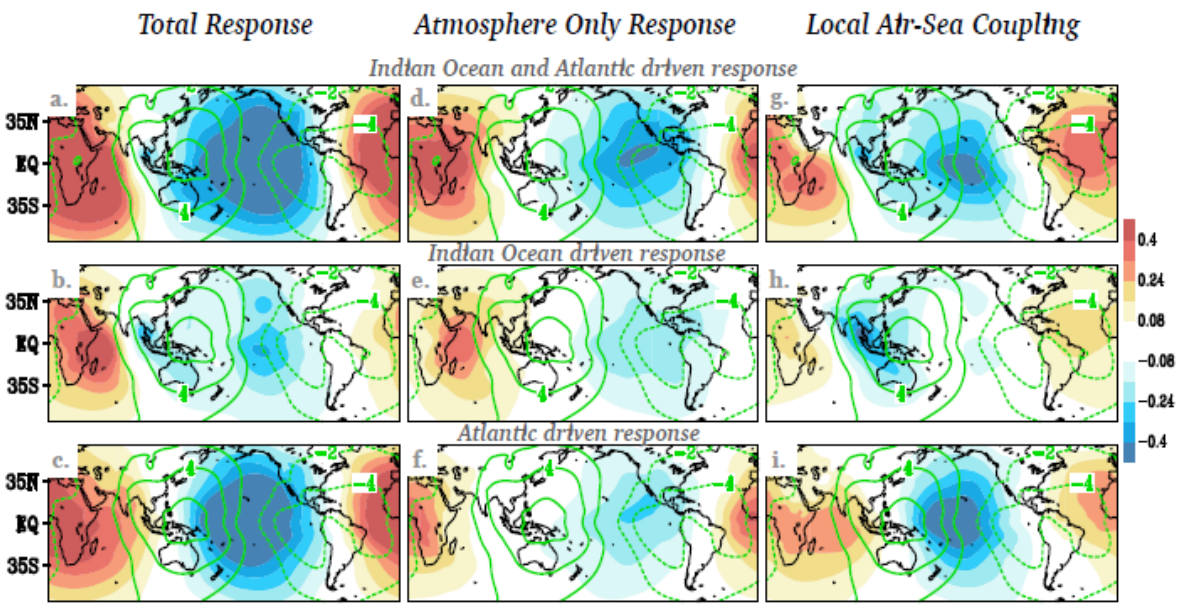

Figure 4. Same as **Fig. 3** but for 850 mb velocity potential (shading, 10^6 m^2 s^{-1}). The climatology of the velocity potential values is superimposed as green contours. Areas of negative (positive) velocity potential indicate regions of strong lower-level divergence (convergence).